Nanoparticle Ordering *via* Functionalized Block Copolymers in Solution

Rastko Sknepnek,[†,*] Joshua A. Anderson,[†] Monica H. Lamm,[‡] Jörg Schmalian,[†] and Alex Travesset[†]

[†]Department of Physics and Astronomy and [‡]Department of Chemical and Biological Engineering, Iowa State University and Ames Laboratory, Ames, Iowa 50011

ARTICLE

ABSTRACT We consider nanoparticles and functionalized copolymers, block copolymers with attached end groups possessing a specific affinity for nanoparticles, in solution. Using molecular dynamics, we show that nanoparticles are able to direct the self-assembly of the polymer/nanoparticle composite. We perform a detailed study for a wide range of nanoparticle sizes and concentrations. We show that the nanoparticles order in a number of distinct phases: simple cubic, layered hexagonal, hexagonal columnar, gyroid, and a novel square columnar. Our results show that nanoparticles ordered with functionalized block copolymers can provide a simple and efficient tool for assembling novel materials with nanometer scale resolution.

KEYWORDS: end-functionalized block copolymers · nanoparticle/copolymer composites · nanoparticle ordering · coarse grained model · molecular dynamics simulation

Block copolymers in solutions or melts are known to self-assemble into mesophases with one-, two-, or three-dimensional periodic order with typical repeating distances in the 10−200 nm range.[1,2] In solutions, the self-assembly of the different phases can be controlled by tuning external conditions such as pH or temperature. The wide availability and relatively inexpensive synthesis of block copolymers as well as the ability to exquisitely control so many diverse phases with periodic order make them compelling candidates for the building blocks of novel materials. Thin films of block copolymers can provide "bottom-up" templates for fabrication of devices on sub-30-nm length scales that are inaccessible to standard lithography techniques, opening the door for molecular size electronic components and ultrahigh density magnetic storage media. Applications include growth of nanowires[3,4] and nanocrystals used in devices such as flash memory,[5] metal-oxide-semiconductor capacitors,[6,7] arrays of quantum dots,[8,9] and photonic crystals.[10] For most applications, the proposed fabrication process consists of forming a thin copolymer film on a substrate, which is then chemically treated to remove one of the copolymer components. The remaining component is used as a mask for growing the active component. It would be even more desirable to include the active component (*e.g.*, metallic or silica nanoparticles) from the outset and form the desired structure in a single pass. Direct application of this method is limited mainly due to nanoparticle aggregation and incompatibility of nanoparticle surface and ionic solutions with the polymers.[11] These problems can be circumvented by the use of self-assembling functionalized block copolymers, that is, polymers with covalently attached end groups that show specific affinity for nanoparticles, as agents for assembling ordered nanoparticle structures.[12,13]

The theoretical understanding of the factors that lead to a successful self-assembly of nanocomposites is relatively limited. Recent studies include investigations of the influence of nanoparticles on the self-assembly and nanostructure formation of diblock copolymer melts based on solving cell dynamical system equations,[14] Monte Carlo simulations,[15] and self-consistent mean field/density functional theory.[16,17] Zhang *et al.*[18] used Brownian dynamics simulations to study the self-assembly of nanoparticles functionalized with oligomeric tethers attached to specific locations on the nanoparticle surface. It is therefore of importance to develop a general framework for predicting how to organize ordered nanoparticle structures. Particularly appealing are bicontinuous triply periodic structures, as they offer optimal topological designs for the maximization of multiple transport properties.[19]

RESULTS AND DISCUSSION

In this contribution, we explore under what conditions functionalized triblock

*Address correspondence to sknepnek@ameslab.gov.

Received for review March 9, 2008 and accepted May 19, 2008.

Published online June 3, 2008.
10.1021/nn8001449 CCC: $40.75

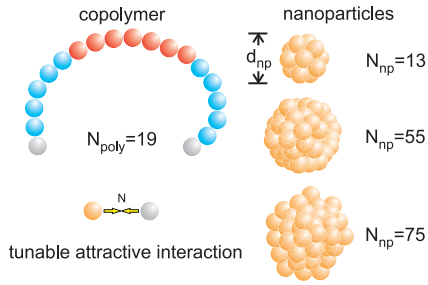

Figure 1. Building block of the coarse grained model. Orange spheres represent the nanoparticle subunits; red (blue) spheres represent hydrophobic (hydrophilic) segments of the copolymer chain. White spheres represent functionalized end groups with tunable affinity, ε_N, for nanoparticles. Each copolymer chain consists of 19 segments, 7 hydrophobic (B) and 12 hydrophilic (A), including 2 end groups ($\tilde{A}$). Nanoparticles are clusters of N_{np} = 13, 55, or 75 units arranged in structures that minimize Lennard-Jones potential.[21] All nanoparticles in a given system are of the same diameter d_{np}. All beads have diameter σ and mass m.

copolymers can be used to successfully assemble ordered nanostructures. Our study is based on the minimal model of functionalized polymers and nanoparticles first introduced in ref 20, now extended to investigate nanoparticle size and shape. The details of the model are summarized in Figure 1. Depending on the nanoparticle concentration, size, and shape, we find a number of two- and three-dimensional ordered structures with distinct nanoparticle ordering: (1) simple cubic, (2) layered hexagonal, (3) hexagonal columnar, (4) gyroid, and (5) square columnar.

We model (Figure 1) the copolymer as a fully flexible harmonic chain of 12 hydrophilic (A) and seven hydrophobic (B) segments of mass m and diameter σ arranged as $\tilde{A}A_5B_7A_5\tilde{A}$ (bead-spring model). $\tilde{A}$ designates two functional end groups which have specific affinity for the nanoparticles; otherwise, segments $\tilde{A}$ are identical to segments A. Each segment represents ≈10 monomers of a real copolymer. Nanoparticles are modeled as a cluster of N_{np} spherical subunits connected with harmonic springs and arranged to minimize Lennard-Jones binding energy.[21] Effects of the solvent are treated implicitly by modifying the interaction between monomers and nanoparticles.

We investigate the phase diagram as a function of nanoparticle affinity ε_N and packing fraction

$$\varphi = \frac{\pi}{6}\frac{nN_{np} + pN_{poly}}{(L/\sigma)^3} \quad (1)$$

where n is the number of nanoparticles, p is the number of copolymers, $N_{poly} = 19$ is the number of segments in each copolymer chain, and L is the length of the simulation box. The relative nanoparticle concentration is

$$c = \frac{nN_{np}}{nN_{np} + pN_{poly}} \quad (2)$$

We first describe the phase diagram for the smallest nanoparticle size studied, $N_{np} = 13$, with an average diameter $d_{np} = 1.2R_g$, where $R_g \approx 2.3\sigma$ is the average radius of gyration of a single copolymer chain. Figure 2 shows the phase diagrams for three relative concentrations of nanoparticles: $c = 0.10$ (a), 0.18 (b), and 0.23 (c) over a range of packing fractions and nanoparticle affinities. For comparison, below each figure, we show the phase diagram of a $A_6B_7A_6$ copolymer system without nanoparticles. Phase boundaries are indicated for clarity only, and the details of the phase diagram calculations are given in the Supporting Information. For low packing fractions $\phi \lesssim 0.2$, no ordering is observed. Polymers form micelles with average aggregation numbers of 10−12 that are in a liquid state. Nanoparticles are unaffected by the polymer and freely diffuse. At weak nanoparticle affinities (ε_N), and as the packing fraction increases, micelles grow in size and solidify in the shape of bent cylinders. Nanoparticles are randomly dispersed without any long-range ordering. We denote this phase as "polydisperse disordered cylinders".

For packing fraction $\phi \gtrsim 0.2$ and nanoparticle affinity $\varepsilon_N/k_BT \gtrsim 1.0$, the system develops two-dimensional order, a square columnar phase (Figure 3). Cylindrical micelles traverse the entire simulation box, and nanoparticles arrange in columns parallel to the micelles.

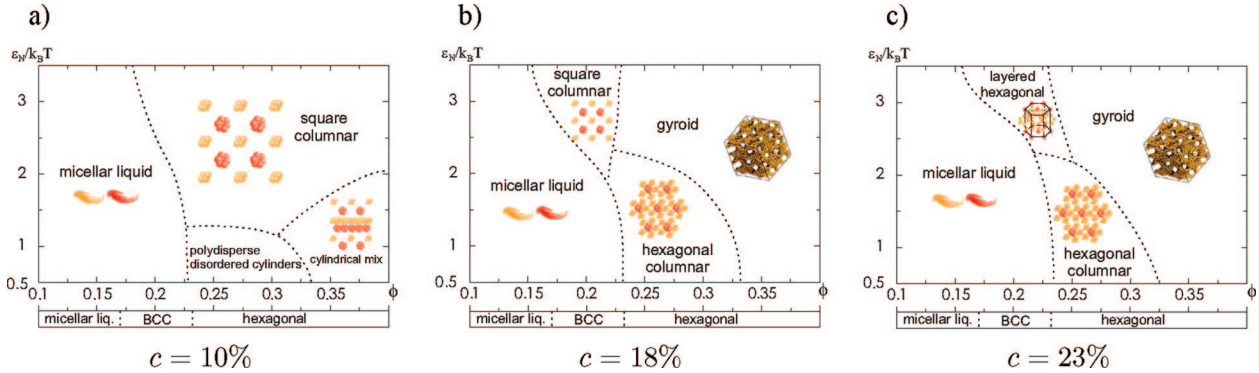

Figure 2. Phase diagram as a function of packing fraction ϕ and nanoparticle−polymer interaction ε_N for the nanoparticle size N_{np} = 13, $d_{np} = 1.2R_g$, and relative concentration of 10% (a), 18% (b), and 23% (c). Phase boundaries (dotted lines) cannot be precisely determined and are indicated for clarity. Lower bar represents phase diagram of $A_6B_7A_6$ copolymer without nanoparticles.[22]

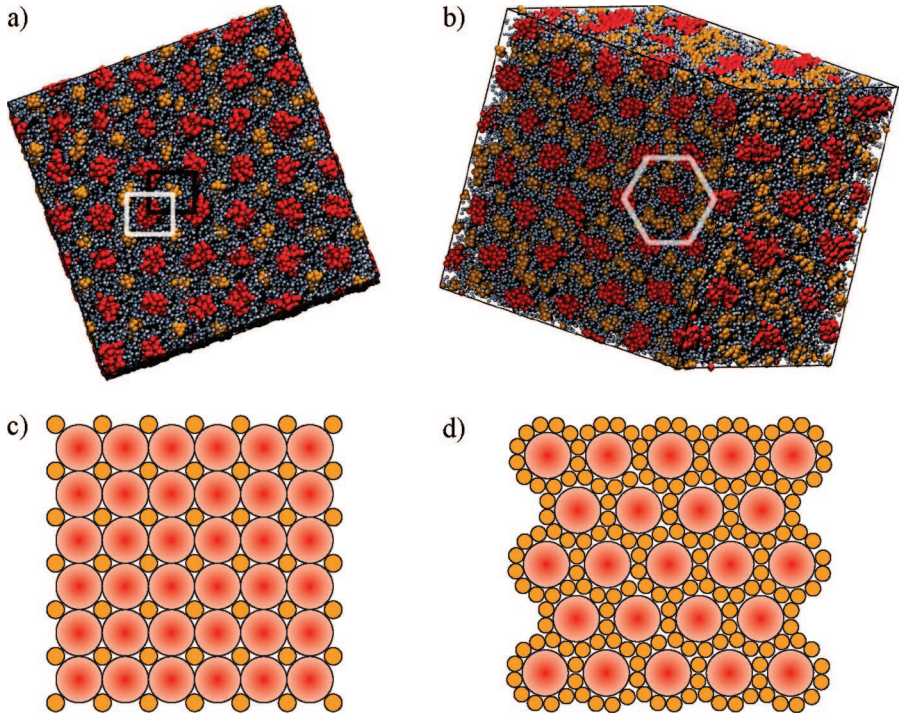

Figure 3. Simulation snapshots of square columnar (a) and hexagonal columnar (b) phases, perpendicular to the cylinders, for systems with 120 (a) and 210 (b) nanoparticles of size $N_{np} = 13$ ($d_{np} = 1.2R_g$) and 600 copolymers, $\varepsilon_N/k_BT = 2.5$ (a) and $\varepsilon_N/k_BT = 1.5$ (b), and packing fraction $\phi = 0.25$. To make ordering more transparent, the snapshots are created with the simulation box replicated two times in each direction. (a) Simulation snapshot of a system in the square columnar phase ($c = 0.13$). Micelles and nanoparticles form two interpenetrating square line-lattices with lattice constant $\approx 9.5\sigma \approx 4.1R_g$; (b) simulation snapshot of a system in the hexagonal columnar phase ($c = 0.205$). Micelles form hexagonal line-lattice with lattice constant $\approx 11.5\sigma \approx 5.0R_g$, and nanoparticles coat them by filling the space between. White and black squares (a) and white hexagon (b) are used to emphasize underlying order. Nanoparticle subunits (orange) and hydrophobic segments (red) are shown at diameter σ. For clarity, hydrophilic (blue) and functionalized end (white) segments are shown at a 50% diameter. (c) Schematic plot of square arrangement of two size disks for size ratio of 0.414214 and 50% relative concentration of small disks.[26,27] (d) Schematic plot of a hexagonal arrangement of two size disks for size ratio 0.349198 and 85.7% relative concentration of small disks.[26,27] All snapshots in this paper are generated with Visual Molecular Dynamics (VMD) package[28] and rendered with Tachyon ray-tracer.[29]

Two interpenetrating square "line-lattices" with equal lattice constants, $a \approx 9.5\sigma \approx 4.1R_g$, are formed. Diffusion is completely suppressed, nanoparticles are well-localized in space, and nanoparticle ordering is successful. In Figure 3a, we show a snapshot of the simulation box perpendicular to the line order emphasizing the square alignment. The square columnar phase is somewhat similar to the ADC phase observed in the lattice Monte Carlo study of the stabilization of ordered bicontinuous phases in diblock copolymer systems.[23] In the "cylindrical mix" region, the square columnar order dissolves in favor of a disordered layered structure formed of cylindrical micelles and nanoparticles stacked in distorted columns, resulting in a failure to form an ordered long-range structure.

As the relative concentration of nanoparticles increases (Figure 2b,c), the square columnar phase is suppressed. At moderate packing fractions, two distinct hexagonal phases emerge. Hexagonal columnar (Figure 3b) is a two-dimensional structure much like the square columnar phase. Cylindrical micelles order in a hexagonal line-lattice with a lattice constant $a \approx 11.5\sigma \approx 5.0R_g$, around 20% larger than the lattice constant of the square columnar phase. The nanoparticles fill in the space between the micellar cylinders, forming a honeycomb-like structure. Both hexagonal and square columnar structures are slightly distorted in the cubic box because their periodic repeat length is not an exact multiple of the box length and thus there is no artificial preference in the system. The issue of the appropriate box size is extensively discussed in ref 22.

The layered hexagonal phase (Figure 4) exhibits three-dimensional order. Spherical micelles form a simple hexagonal lattice, while nanoparticles arrange in perforated layers located between the micellar planes. The resulting structure resembles that of $CaCu_5$, with the important difference that there are no nanoparticles in the layer occupied by micelles.

For large packing fractions, the system orders into a gyroid phase (Figure 6). The polymer forms a centrosymmetric gyroid, imposing the same order onto the nanoparticles. Both gyroids possess the $Ia\bar{3}d$ space group symmetry,[25] as confirmed by the structure factor calculation (Figure 7) for nanoparticles and hydrophobic segments.

If the nanoparticle size is increased to $N_{np} = 55$ (nearly spherical, $d_{np} = 2.1R_g$) and $N_{np} = 75$ (slightly oblong largest available Lennard-Jones cluster,[21] $d_{np} =$

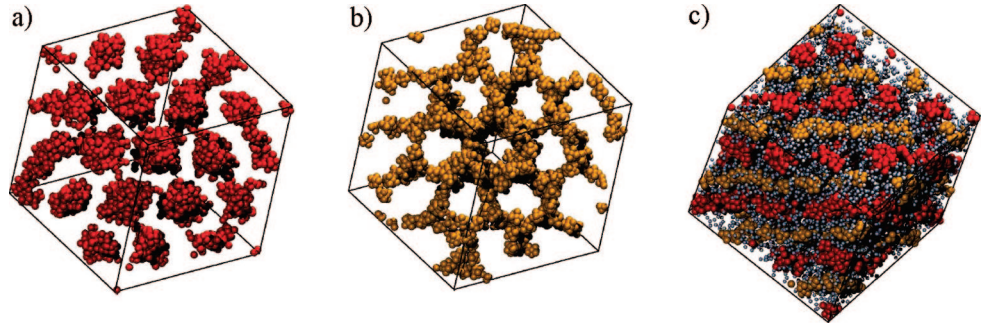

Figure 4. Layered hexagonal phase. A view of a simulation snapshot for the system with 240 nanoparticles (N_{np} = 13) and 600 copolymers (c = 0.23), nanoparticle affinity ε_N/k_BT = 1.5, and packing fraction ϕ = 0.35. Hydrophobic segments (red) from a simple hexagonal lattice (a) (top view); for presentation purposes, we omit hydrophilic segments. Nanoparticles (orange) form perforated layers resembling a honeycomb (b) (top view), placed between micellar layers (c) (side view). In the right-hand side figure, hydrophilic (blue) and terminal (white) segments are shown at a 50% radius.

$2.5R_g$ along the longest axis), the nanoparticle ordering remains successful (Figure 5a). The square columnar phase (Figure 5b) stabilizes for large packing fractions and weak to moderate nanoparticle affinities. The gyroid phase is pushed toward higher values of ϕ and ε_N/k_BT. For packing fractions, $\phi \approx 0.15-0.3$ and $\varepsilon_N/k_BT \gtrsim 2$, a new three-dimensional ordered structure appears. Nanoparticles are successfully ordered in a simple cubic lattice with lattice constant $a \approx 9.5\sigma \approx 4.1R_g$. The full ordered structure is a CsCl lattice where spherical micelles and nanoparticles form two interpenetrating cubic lattices, that is, each nanoparticle is surrounded by eight equidistant micelles and *vice versa*.

Our results show that functionalized copolymers can be successfully used to assemble ordered structures of nanoparticles. Although the order will be mainly dictated by the polymer subsystem, the nanoparticles are not silent observers but direct the process of structure formation, either by stabilizing the polymer order (in the case of the gyroid phase) or by significantly rearranging micelles (in the case of square columnar phase).

To clarify the origin of the two-dimensional ordered structures, square columnar and cylindrical hexagonal, we resort to an analogy with the packing problem of two size disks, extensively studied in discrete mathematics.[26,27] For comparison, packing of two size disks with the closest resemblance to the structures observed in our simulations are shown in Figure 3c,d. Optimal packing depends on the relative concentration and size ratio of two disks. Dependence on the relative concentration is apparent in transition from Figure 2a to Figure 2b to Figure 2c. As the relative number of nanoparticles increases, the square columnar phase is replaced with the cylindrical hexagonal and layered hexagonal, depending on packing fraction and nanoparticle affinity. The ratio between nanoparticle radius and the radius of a micellar cylinder plays the role of the relative size of two disks. For example, in the case shown in Figure 3a, the nanoparticle (micelle) diameter is $d_{np} = 1.2R_g$ ($d_{mic} \approx 4.5R_g$), with the size ratio ≈0.27, roughly one-half of the size ratio for disks shown in Figure 3c. At a quantitative level, the analogy be-

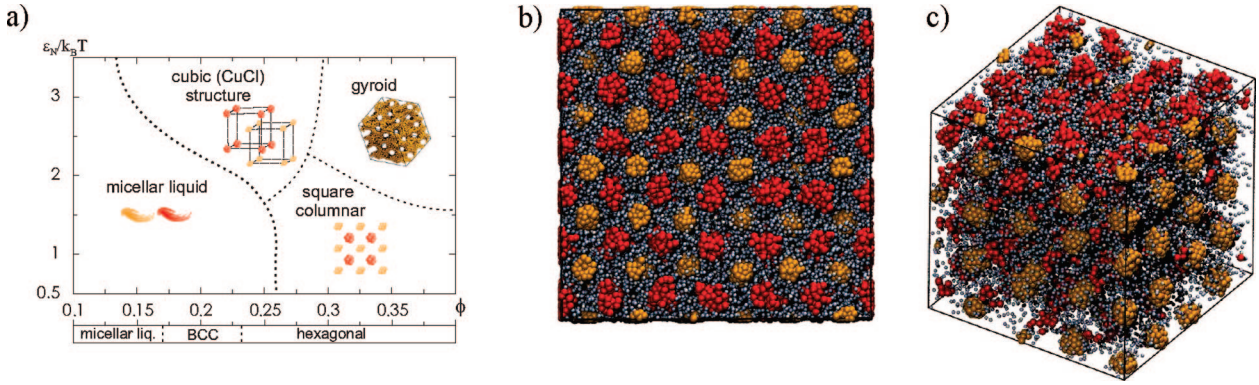

Figure 5. (a) Phase diagram for the relative concentration of 21% of the largest available (N_{np} = 75, $d_{np} = 2.5R_g$) nanoparticles as the function of packing fraction ϕ and interaction strength ε_N/k_BT. Ordered nanoparticle structures are observed in the wide portion of the phase diagram with three distinct ordered phases: simple cubic, square columnar, and gyroid. Lower bar represents phase diagram of $A_6B_7A_6$ copolymer without nanoparticles. (b) Simulation snapshot of the square columnar phase with 40 nanoparticles (N_{np} = 75, $d_{np} = 2.5R_g$) and 600 copolymers for ϕ = 0.3 and ε_N/k_BT = 1.5. Nanoparticle subunits (orange) and hydrophobic segments (red) are shown at diameter σ. Simulation box is replicated two times in each direction. (c) Simulation snapshot of cubic phase with 64 nanoparticles (N_{np} = 75, $d_{np} = 2.5R_g$) and 910 copolymers for ϕ = 0.2 and ε_N/k_BT = 2.5. For clarity, hydrophilic (blue) and terminal (white) segments are shown at a 50% diameter, (b) and (c).

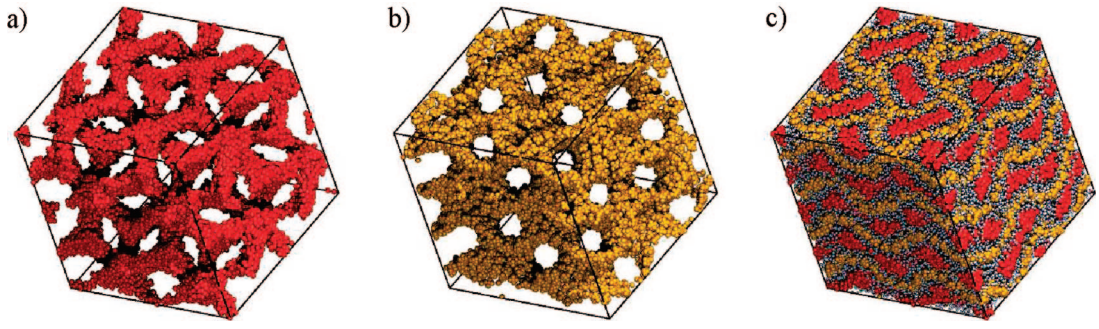

Figure 6. Gyroid phase. A view of a simulation snapshot for the system with 270 nanoparticles ($N_{np} = 13$, $d_{np} = 1.2R_g$) and 600 copolymers ($c = 0.25$), nanoparticle affinity $\varepsilon_N/k_BT = 1.5$, and packing fraction $\phi = 0.35$. Hydrophobic part (red) of copolymer chains from a centrosymmetric gyroid (a); for presentation purposes, we omit hydrophilic segments. Nanoparticles (orange) also form a gyroid with the same symmetry (b). The two gyroids interpenetrate each other (c). In the right-hand side figure, hydrophilic (blue) and terminal (white) segments are shown at a 50% radius. For clarity, the snapshots are created with the simulation box replicated two times in each direction.

tween the optimal packing of disks and nanoparticle ordering must be taken with some caution, as the functional polymer end groups provide a favorable energy for nanoparticles, which goes beyond the hard disk interactions assumed in the optimal disk packing.

Effects of nanoparticle affinity become even more important as the nanoparticle size is increased. More functional end groups can simultaneously attach to a single nanoparticle, effectively increasing the attractive interaction. This effect is most prominent in the case of cubic structures. A cubic lattice has low density and coordination compared to close packed structures, and its formation depends intricately on the details of the interaction potential.[30]

For large packing fractions and nanoparticle affinities, we find a gyroid phase. Transition to the gyroid phase can be explained as follows. With an increase in density, micelles start to merge as hydrophobic segments tend to minimize contact with the solvent. The system also prefers to minimize surface tension of the layer connecting hydrophobic and hydrophilic segments, which can be achieved by reducing the curvature of the contact surface. As a result a minimal surface—a gyroid—forms. A somewhat similar scenario has been reported for selective nanoparticles in diblock melts.[31] Nanoparticles fill the space surrounding the micellar gyroid, forming a complementary gyroid structure. It, however, appears that nanoparticles help stabilize gyroid order since even significantly smaller nanoparticles ($N_{np} = 1$, $d_{np} = 0.4R_g$)[20] than those considered here notably extend the region of parameter space occupied by the gyroid phase.

Using a minimal coarse grained model for nanoparticles in a solution of triblock copolymers with functionalized end groups, we have mapped the phase diagram over a wide range of nanoparticle sizes, concentrations, and packing fractions. We find a rich phase diagram with five phases containing distinct long-range nanoparticle order: (1) square columnar, (2) hexagonal columnar, (3) layered hexagonal, (4) cubic, and (5) gyroid. We showed that nanoparticle order can be controlled by changing relative size, concentration, and affinity between nanoparticles and copolymers.

A good candidate for the experimental realization of the proposed nanocomposite assembly strategy is, commercially available, Pluronic triblock copolymer. Functionalizing Pluronics by covalently attaching end groups with different chemical properties is a topic of intense research, and a number of successful attempts have already been made. For example, Pluronic F127 and the poly(2-diethylaminoethyl methacrylate), PDEAEM, modified Pluronic F127 ($PDEAEM_{35}$-F127-$PDEAEM_{35}$)[32] pentablock copolymers have been functionalized with 14 amino acid hydroxyapatite binding peptides and successfully used to template 5−10 nm calcium phosphate nanoparticles.[12,13] Further, experiments with growing magnetite nanoparticles in an or-

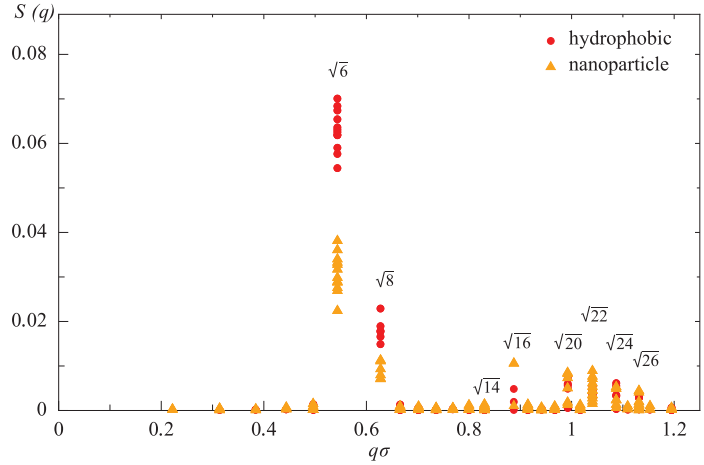

Figure 7. Structure factor in the gyroid phase for a system with 270 nanoparticles and 600 copolymers ($c = 0.25$), nanoparticle affinity $\varepsilon_N/k_BT = 1.5$, and packing fraction $\phi = 0.35$. Peaks corresponding to the position of hydrophobic segments are represented with the red circles. Orange triangles are peaks corresponding to the position of nanoparticles. Square roots above peaks designate peaks allowed by the $Ia\bar{3}d$ space group.[25] Note that $\sqrt{14}$ is essentially indistinguishable from the noise.

ganic matrix made of Pluronic F127 copolymer with covalently attached MMS6 protein, found in magnetotactic bacteria,[33] suggest that the morphology and alignment of the formed nanocrystals could be successfully controlled by the underlying organic matrix.[34,35]

MODEL AND SIMULATION DETAILS

We use a generic triblock copolymer modeled with a bead-spring model of $N_{poly} = 19$ segments arranged as $\tilde{A}A_5B_7A_5\tilde{A}$. Segments ($A$) are hydrophilic while segments (B) are hydrophobic. Two terminal segment ($\tilde{A}$) are functionalized to show affinity for nanoparticles; otherwise, they are identical to the remaining segments of type A. This is, for example, a suitable coarse grained representation of a Pluronic polymer. In this model, each segment represents approximately 10 Kuhn monomers of a real polymer. Effects of the solvent are included implicitly through the effective nonbonding interactions. The nonbonded interactions are described as effective Lennard-Jones potentials. Following ref 24, we choose

$$V_{ij}(r) = 4\varepsilon_{ij}\left[\left(\frac{\sigma}{r}\right)^{12} - \alpha_{ij}\left(\frac{\sigma}{r}\right)^{6}\right] \quad (3)$$

where

$$\alpha_{ij} = \begin{cases} 1 & i,j = B \\ 0 & \text{otherwise} \end{cases}$$

σ is the Lennard-Jones radius, and ε_{ij} is the interaction energy. All bond angle and torsion interactions are ignored. The bonded interactions are modeled with the simple harmonic potential $U(r) = 1/2k(r - r_0)^2$, with $k = 330\varepsilon\sigma^{-2}$, and $r_0 = 0.9\sigma$. Note that all quantities are measured in reduced Lennard-Jones units, that is, distances are measured in unit of σ and energies in units of ε/k_BT.

Nanoparticles are modeled as clusters of N_{np} subunits held together by a harmonic potential $U(r) = 1/2k_{np}(r - r_0)^2$, where $r_0 = 0.9\sigma$ and $k_{np} = 330\varepsilon\sigma^{-2}$. Each subunit is connected to its nearest neighbors such that the overall shape of the nanoparticle is preserved. The positions of subunits within a nanoparticle are chosen to form a minimum Lennard-Jones energy cluster of N_{np} subunits.[21] Within each run, nanoparticles are monodisperse. Simulations are performed with three nanoparticle sizes, $N_{np} = 13$, 55, and 75 with the average diameter, $d_{np} = 1.2R_g$, $2.1R_g$, and $2.5R_g$ (along the longest axis), respectively. ($R_g \approx 2.3\sigma$ is the average radius of gyration of a single copolymer chain calculated for parameter values of the full simulation, *i.e.*, $\alpha_{AA} = \alpha_{AB} = 0$, $\alpha_{BB} = 1$, $\varepsilon/k_BT = 1.0$, $k = 330\varepsilon\sigma^{-2}$, $r_0 = 0.9\sigma$, and reduced temperature $T = 1.2$.) The first two sizes are chosen as they are are almost spherical, while the last one is the largest available Lennard-Jones cluster and is slightly oblong. Note that in our model nanoparticles are not rigid, and their average size fluctuates. These size fluctuations are very small ($\Delta d_{np} \propto \sqrt{(2k_BT/k_{np})} \approx 0.08\sigma$) and can be safely neglected.

Interaction between different nanoparticles is assumed to be repulsive and modeled as

$$V_{NN}(r) = 4\tilde{\varepsilon}\left(\frac{\sigma}{r}\right)^{12} \quad (4)$$

Interaction between nanoparticles and copolymers is modeled with an attractive potential

$$V_{N\tilde{A}}(r) = 4\varepsilon_N\left[\left(\frac{\sigma}{r}\right)^{12} - \left(\frac{\sigma}{r}\right)^{6}\right]$$

between the functional end groups ($\tilde{A}$) and nanoparticle subunits with a tunable strength ε_N. The rest of the copolymer chain is repelled from nanoparticles with an $\propto r^{-12}$ potential.

Simulations are performed with LAMMPS simulation package.[36] Masses of all beads are set to $m = 1$, Lennard-Jones radius to $\sigma = 1$, and interaction strengths $\varepsilon_{ij} = \tilde{\varepsilon} = 1$ (*cf.* eqs 3 and 4). We consider a fixed number $p = 600$ and 1000 of polymers in a cubic box of length L subject to the periodic boundary conditions.

Relative nanoparticle concentration is calculated as the ratio of the nanoparticle beads to the total number of beads

$$c = \frac{nN_{np}}{nN_{np} + pN_{poly}}$$

where n is the number of nanoparticles. Simulations are performed for seven values of the relative nanoparticle concentration $c = 0.09$, 0.12, 0.146, 0.17, 0.193, 0.215, and 0.235 for $N_{np} = 13$ size nanoparticle, $c = 0.126$, 0.162, 0.178, 0.194, 0.224, 0.30, and 0.37 for $N_{np} = 55$ size nanoparticle, and one value of relative nanoparticle concentration $c = 0.208$ for the $N_{np} = 75$ size nanoparticle. Nanoparticle affinity ε_N/k_BT is tuned from 1.0 to 3.0 with a 0.5 step. All simulations are performed for five total densities (volume fractions) $\rho = (nN_{np} + pN_{poly})/L^3$ ($\phi = \pi/6\rho$), $\rho(\phi) = 0.28648(0.15)$, 0.38197(0.20), 0.47746(0.25), 0.57296(0.3), and 0.66845(0.35). All runs are performed in the NVT ensemble at a reduced Lennard-Jones temperature $T = 1.2$.[37] Depending on the parameters, simulations are carried over 10 to 20 million time steps with a step size $\Delta\tau = 0.005\tau$ ($\tau = \sqrt{(m\sigma^2/\varepsilon)}$ being the unit of dimensionless time). Snapshots of the simulation are recorded every 10^4 time steps starting after the 5 millionth time step, which is well beyond a typical $\tau_{eq} \approx 2 \times 10^6$ time steps it took to equilibrate even the largest system sizes at highest concentrations. In order to ensure that our simulations are not locked in metastable phases but reach an equilibrium state, we have selected at random a number of points in the phase diagram and repeated simulations starting from different random initial configurations. Our confidence that these are true equilibrium structures is further enhanced by the fact that the ordered phases form within the first million time steps and stay stable for more than 50 million time steps, as confirmed by a few extremely long ($\sim 10^8$ time steps) test runs.

The initial configurations are built in a two-step process: (1) n nanoparticles are placed at random positions and given random orientations, (2) p polymer chains are grown using self-avoiding random walkers. This scheme works well for low densities up to $\approx$0.5. Simulations at the two largest densities, 0.57296 and 0.66845, are initiated with $\rho = 0.47746$ initial configurations. Then, using the LAMMPS *rescale* command over 5 million time steps, the simulation box is gradually shrunk until the desired density is achieved. To ensure reproducibility, each run was performed from a different initial configuration. The total time required to run the simulations presented in this paper is approximately 10 CPU years on a single AMD Opteron 2.4 GHz processor.

Acknowledgment. We acknowledge many useful discussions with L. Filion, M. Kanapathipillai, S. K. Mallapragada, B. Narasimhan, M. Nilsen-Hamilton, R. Prozorov, and T. Prozorov. This research was supported by the U.S. Department of Energy Grant DE-AC02-07CH11358 and partially by the NSF Grant DMR-0426597 (J.A. and A.T.).

Supporting Information Available: Structure factor for the gyroid phase and detailed data points for the determination of the phase diagram. This material is available free of charge *via* the Internet at http://pubs.acs.org.

REFERENCES AND NOTES

1. Alexandridis, P., Lindeman, B., Eds. *Amphiphilic Block Copolymers: Self-Assembly and Applications*; Elsevier Science: Amsterdam, 2000.
2. Matsen, M. The Standard Gaussian Model for Block Copolymer Melts. *J. Phys.: Condens. Matter* **2002**, *14*, R21−R48.
3. Thurn-Albrecht, T.; Schotter, J.; Kästle, G. A.; Emley, N.; Shibauchi, T.; Krusin-Elbaum, L.; Guarini, K.; Black, C. T.; Tuominen, M. T.; Russell, T. P. Ultrahigh-Density Nanowire Arrays Grown in Self-Assembled Diblock Copolymer Templates. *Science* **2000**, *290*, 2126–2129.
4. Lopes, W. A.; Jaeger, H. M. Hierarchical Self-Assembly of Metal Nanostructures on Diblock Copolymer Scaffolds. *Nature* **2001**, *414*, 735–738.
5. Guarini, K. W. ; Black, C. T. ; Zhang, Y. ; Babich, I. V. ; Sikorski, E. M. ; Gignac, L. M. Low Voltage, Scalable Nanocrystal FLASH Memory Fabricated by Templated Self-Assembly. In *International Electron Devices Meeting Technical Digest*; 2003, pp 22.2.1−22.2.4.
6. Black, C. T.; Guarini, K. W.; Milkove, K. R.; Baker, S. M.; Russell, T. P.; Tuominen, M. T. Integration of Self-Assembled Diblock Copolymers for Semiconductor Capacitor Fabrication. *Appl. Phys. Lett.* **2001**, *79*, 409–411.
7. Black, C. T.; Guarini, K.W.; Ying, Z.; Hyungjun, K.; Benedict, J.; Sikorski, E.; Babich, I. V.; Milkove, K. R. Polymer Self-Assembly in Semiconductor Microelectronics. *IEEE Electron Device Lett.* **2004**, *25*, 622–624.
8. Park, M.; Harrison, C.; Chaikin, P. M.; Register, R. A.; Adamson, D. H. Block Copolymer Lithography: Periodic Arrays of $\sim 10^{11}$ Holes in 1 Square Centimeter. *Science* **1997**, *276*, 1401–1404.
9. Li, R. R.; Dapkus, P. D.; Thompson, M. E.; Jeong, W. G.; Harrison, C.; Chaikin, P. M.; Register, R. A.; Adamson, D. H. Dense Arrays of Ordered GaAs Nanostructures by Selective Area Growth on Substrates Patterned by Block Copolymer Lithography. *Appl. Phys. Lett.* **2000**, *76*, 1689–1691.
10. Urbas, A.; Sharp, R.; Fink, Y.; Thomas, E. L.; Xenidou, M.; Fetters, L. J. Tunable Block Copolymer/Homopolymer Photonic Crystals. *Adv. Mater.* **2000**, *12*, 812–814.
11. Pozzo, D. C.; Walker, L. M. Small-Angle Neutron Scattering of Silica Nanoparticles Templated in PEO-PPO-PEO Cubic Crystals. *Colloids Surf. A* **2007**, *294*, 117–129.
12. Enlow, D.; Rawal, A.; Kanapathipillai, M.; Schmidt-Rohr, K.; Mallapragada, S.; Lo, C.-T.; Thiyagarajan, P.; Akinc, M. Synthesis and Aharacterization of Self-Assembled Block Copolymer Templated Calcium Phosphate Nanocomposite Gels. *J. Mater. Chem.* **2007**, *17*, 1570–1578.
13. Kanapathipillai, M.; Rawal, A.; Yusufoglu, Y.; Hu, Y.-Y.; Lo, C.-T.; Thiyagarajan, P.; Kalay, Y. E.; Akinc, M.; Mallapragada, S.; Schmidt-Rohr, K. Synthesis and Characterization of Ionic Block Copolymer Templated Calcium Phosphate Nanocomposites. *Chem. Mater.* **2008**, in press.
14. Ginzburg, V. V.; Gibbons, C.; Qiu, F.; Peng, G.; Balazs, A. C. Modeling the Dynamic Behavior of Diblock Copolymer/Particle Composites. *Macromolecules* **2000**, *33*, 6140–6147.
15. Huh, J.; Ginzburg, V. V.; Balazs, A. C. Thermodynamic Behavior of Particle/Diblock Copolymer Mixtures: Simulation and Theory. *Macromolecules* **2000**, *33*, 8085–8096.
16. Thompson, R. B.; Ginzburg, V. V.; Matsen, M. W.; Balazs, A. C. Block Copolymer-Directed Assembly of Nanoparticles: Forming Mesoscopically Ordered Hybrid Materials. *Macromolecules* **2002**, *35*, 1060–1071.
17. Pryamitsyn, V.; Ganesan, V. Strong Segregation Theory of Block Copolymer-Nanoparticle Composites. *Macromolecules* **2006**, *39*, 8499–8510.
18. Zhang, Z. L.; Horsch, M. A.; Lamm, M. H.; Glotzer, S. C. Tethered Nano Building Blocks: Toward a Conceptual Framework for Nanoparticle Self-Assembly. *Nano Lett.* **2003**, *3*, 1341–1346.
19. Torquato, S.; Hyun, S.; Donev, A. A. Multifunctional Composites: Optimizing Microstructures for Simultaneous Transport of Heat and Electricity. *Phys. Rev. Lett.* **2002**, *89*, 266601-1–266601-4.
20. Knorowski, C. D.; Anderson, J. A.; Travesset, A. Self-Assembled Ordered Polymer Nanocomposites Directed by Attractive Particles. *J. Chem. Phys.* **2008**, *128*, 164903–164907.
21. Sloane, N. J. A.; Hardin, R. H.; Duff, T. S.; Conway, J. H. Minimal-Energy Clusters of Hard Spheres. *Discrete Comput. Geom.* **1995**, *14*, 237–259.
22. Anderson, J. A.; Lorenz, C. D.; Travesset, A. Micellar Crystals in Solution from Molecular Dynamics Simulations. *J. Chem. Phys.* **2008**, *128*, 184906–184917.
23. Martínez-Veracoechea, F. J.; Escobedo, F. A. Monte Carlo Study of the Stabilization of Complex Bicontinuous Phases in Diblock Copolymer Systems. *Macromolecules* **2007**, *40*, 7354–7365.
24. Anderson, J. A; Travesset, A. Coarse-Grained Simulations of Gels of Nonionic Multiblock Copolymers with Hydrophobic Groups. *Macromolecules* **2006**, *39*, 5143–5151.
25. Hajduk, D. A.; Harper, P. E.; Gruner, S. M.; Honeker, C. C.; Gia, K.; Thomes, E. L.; Fetters, L. J. The Gyroid: A New Equilibrium Morphology in Weakly Segregated Diblock Copolymers. *Macromolecules* **1994**, *27*, 4063–4075.
26. Fejes Tóth, L. *Regular Figures*; The Macmillan Company: New York, 1964.
27. Uche, O. U.; Stillinger, F. H.; Torquato, S. Concerning Maximal Packing Arrangements of Binary Disk Mixtures. *Physica A* **2004**, *342*, 428–446.
28. Humphrey, W.; Dalke, A.; Schulten, K. VMD—Visual Molecular Dynamics. *J. Mol. Graphics* **1996**, *14*, 33–38.
29. Stone, J. *An Efficient Library for Parallel Ray Tracing and Animation*; Computer Science Department: University of Missouri—Rolla, 1998.
30. Rechtsman, M. C.; Stillinger, F. H; Torquato, S. Self-Assembly of the Simple Cubic Lattice with an Isotropic Potential. *Phys. Rev. E* **2007**, *74*, 021404–021411.
31. Kim, B.; Fredrickson, G. H.; Hawker, C. J.; Kramer, E. J. Nanoparticle Surfactants as a Route to Bicontinuous Block Copolymer Morphologies. *Langmuir* **2007**, *23*, 7804–7809.
32. Determan, M. D.; Cox, J. P.; Seifert, S. Synthesis and Characterization of Temperature and pH-Responsive Pentablock Copolymers. *Polymer* **2005**, *46*, 6933–6946.
33. Arakaki, A; Webb, J.; Matsunaga, T. A Novel Protein Tightly Bound to Bacterial Magnetic Particles in Magnetospirillum Magneticum Strain AMB-1. *J. Biol. Chem.* **2003**, *278*, 8745–8750.
34. Prozorov, T; Mallapragada, S. K.; Narasimhan, B; Wang, L; Palo, P; Nilsen-Hamilton, M; Williams, T. J.; Bazylinski, D. A.; Prozorov, R.; Canfield, P. C. Protein-Mediated Synthesis of Uniform Superparamagnetic Magnetite Nanocrystals. *Adv. Funct. Mater.* **2007**, *17*, 951–957.
35. Prozorov, R; Prozorov, T.; Mallapragada, S. K.; Narasimhan, B.; Williams, T. J.; Bazylinsky, D. A. Magnetic Irreversibility and the Verwey Transition in Nanocrystalline Bacterial Magnetite. *Phys. Rev. B* **2007**, *76*, 054406-1–054406-9.
36. Plimpton, S. Fast Parallel Algorithms for Short-Range Molecular Dynamics. *J. Comput. Phys.* **1995**, *117*, 1–19.
37. Rapaport, D. *The Art of Molecular Dynamics Simulation*, 2nd ed.; Cambridge University Press: Cambridge, 2004.